JOURNAL OF MATERIALS SCIENCE 26 (1991) 3067–3072

Fragmentation of brittle materials at high rates of loading

J. LANKFORD, C. R. BLANCHARD
Materials and Mechanics Department, Southwest Research Institute, San Antonio, TX78228-0510, USA

Experiments involving the fragmentation of SiC during both quasistatic and high-rate compressive loading are described. Measured fragment size distributions are considered in terms of current ideas regarding high strain rate damage and microfracture. It is concluded that both crack dynamics and crack nucleation via plastic flow mechanisms may be important elements in the failure process.

1. Introduction

The fragmentation of brittle materials has a wide range of physical relevance including, but not limited to, such phenomena as rock comminution, the milling of powders, hard particle impact of ceramic and ceramic composite structures, and the penetration of ceramic armour. In many of these cases, fragments are produced under conditions which generate high rates of compressive loading. The actual process of dynamic fragmentation is not well understood, but earlier theoretical and experimental efforts provide useful insight regarding the factors which probably are involved. In order to support the subsequent interpretation of the experiments described in this paper, it is useful to consider briefly the relevant background.

Generally, brittle materials fail by means of crack nucleation and growth, with no preceding or attendant plastic flow; under compressive loading, failure consists of the eventual coalescence of a multitude of microcracks. Because it is these microcracks which produce the observed post-failure fragments, it is clear that the average fragment size is directly related to the average crack size at coalescence. The dependence of fragment size on material properties and strain rate has been considered theoretically by Grady and Kipp in a series of papers [1–3]. As they observe, it is possible to analyse the fragmentation process from at least two points of view, i.e. inherent flaws and energy balance, and they recently have been able to reconcile these seemingly variant treatments.

In particular, it can be shown directly, by balancing kinetic (elastic expansion) and potential (fracture surface) energies, that for brittle fracture the average fragment size can be described explicitly by [3]

$$\bar{d} = \left(\frac{20^{1/2} K_{IC}}{\rho c \dot{\varepsilon}_f}\right)^{2/3} \quad (1)$$

where K_{IC} is the fracture toughness, ρ is the density, c is the elastic wave speed, and $\dot{\varepsilon}_f$ is the applied strain rate at failure. From equilibrium energy theory [1], it is possible to conclude that if this relationship holds, the number of flaws, N, which activates at a (local) tensile* stress, σ, should, in order to achieve an equilibrium surface area, increase at least as rapidly as

$$N \propto \sigma^6 \quad (2)$$

Alternatively, from the inherent flaw point of view [2], it is possible to develop an expression for a strain rate-dependent fracture stress, i.e.

$$\sigma_c = f(k, m, c, E)\dot{\varepsilon}_f^{3/(m+3)} \quad (3)$$

where f is a function of the material constants k, m, c, and E (the elastic modulus); k and m are defined through a two-parameter Weibull law of the form

$$N = k\sigma^m \quad (4)$$

Because Equation 2 requires $m \gtrsim 6$, it follows from Equation 3 that if energy-balance equilibrium prevails, the fracture stress should follow

$$\sigma_c \propto \dot{\varepsilon}^{1/3} \quad (5)$$

In the absence of equilibrium, m will be < 6, and the strain rate exponent in Equation 5 will be higher than 1/3.

An alternative view to the crack dynamics approach has been provided by Janach [4, 5], who noted that high stress rates generate uniaxial strain conditions, hence, transient confining pressures of maximum theoretical value equal to about one third of the axial stress. To realize this high level of confinement, it generally is assumed the loading is basically a step (shock) pulse, so that the specimen has little time to relax radially via Poisson expansion. It should be noted that while this condition requires higher failure stresses, it represents no fundamental departure from the quasistatic microfracture process, i.e. no significant alteration in fragment size is implicated.

Finally, several studies [6–10] have addressed the notion of whether there exists a minimum fragment size which can be attained. The basic problem is that

*Compressively loaded brittle materials actually fail in tension at a multiplicity of sites at which the global compressive stress field is resolved into highly localized tensile enclaves.

0022–2461/91 $03.00 + .12 © *1991 Chapman and Hall Ltd.*

in breaking up particles, a critical size is reached below which further fragmentation is seemingly impossible because the particles begin to flow plastically. However, the consequences of plastic flow in ceramics with regard to microfracture have been explored by Hagan [11], who was interested in crack formation within constrained plastic zones beneath microhardness indentations. Here, stresses can be very high, a situation which also should prevail in bulk test specimens at high strain rates (Equation 5). It will be shown that under these conditions, fragments significantly smaller than those predicted by Equation 1 would be anticipated.

2. Experimental procedure

The compression testing procedures have been described previously [12], and so are outlined here only briefly. Right circular cylindrical specimens of sintered alpha silicon carbide were ground parallel within 4 μm, and lapped with diamond polishing compound to remove residual surface damage. They were compressed to failure between similarly prepared high-strength alumina loading platens, at strain rates of 10^{-5}, 1.0, and 2200 s^{-1}. The latter rate was achieved by means of the split Hopkinson pressure bar, and defined as the maximum stress rate of the loading pulse generated within the specimen divided by its elastic modulus.

For each test, the resulting particulate debris was contained within flexible plastic enclosures wrapped about the platens; the fragments thus captured were then suspended in ethanol to achieve complete and random spatial dispersion. A sample drawn by eye dropper from this suspension was placed on a glass slide, dried, and finally gold-coated. In order to establish the relative sizes of the fragments, all of the particles on each slide were imaged via scanning electron microscope, and characterized by a computer-controlled image-analysing system. In no case were less than 2500 particles characterized. The resulting area-based fragment size distribution was computed in terms of per cent particle frequency against projected area-equivalent particle diameter.

Relevant material properties for the SiC are listed in Table I.

3. Results

The relationship between fragment size, d, and compressive strain rate, $\dot{\varepsilon}$, is shown in Fig. 1. At a strain rate of 10^{-5} s^{-1}, the size distribution is skewed toward the high end, and in fact, a few gross (fraction of a millimeter) particles do not even manifest themselves in this presentation. The distributions for $\dot{\varepsilon} = 1$ s^{-1} and 2.2×10^3 s^{-1} are more sharply peaked; in all three cases, separation between the peaks is evident. A typical high strain-rate fragment is shown in Fig. 2.

The peak values, $\bar{d}$, are plotted in Fig. 3 against strain rate; also shown are the corresponding compressive strengths, σ_c. Based on previous SiC results, as well as the predictions (Equation 5) of dynamic fracture models [2, 13], a line of slope equal to one-third has been drawn through the high-rate strength data. Similarly, the fragment size at $\dot{\varepsilon} = 2.2 \times 10^3$ s^{-1} is shown against the relationship (Equation 1) predicted on the basis of dynamic fracture considerations. It is evident that the experimental result ($\bar{d} = 3$ μm) is somewhat lower than the predicted one, but far below the value which would be expected by extrapolating the lower strain rate data.

TABLE I Material properties

Elastic modulus (GPa)	Fracture toughness (MPa $m^{1/2}$)	Poisson's ratio
380	4.0	0.21

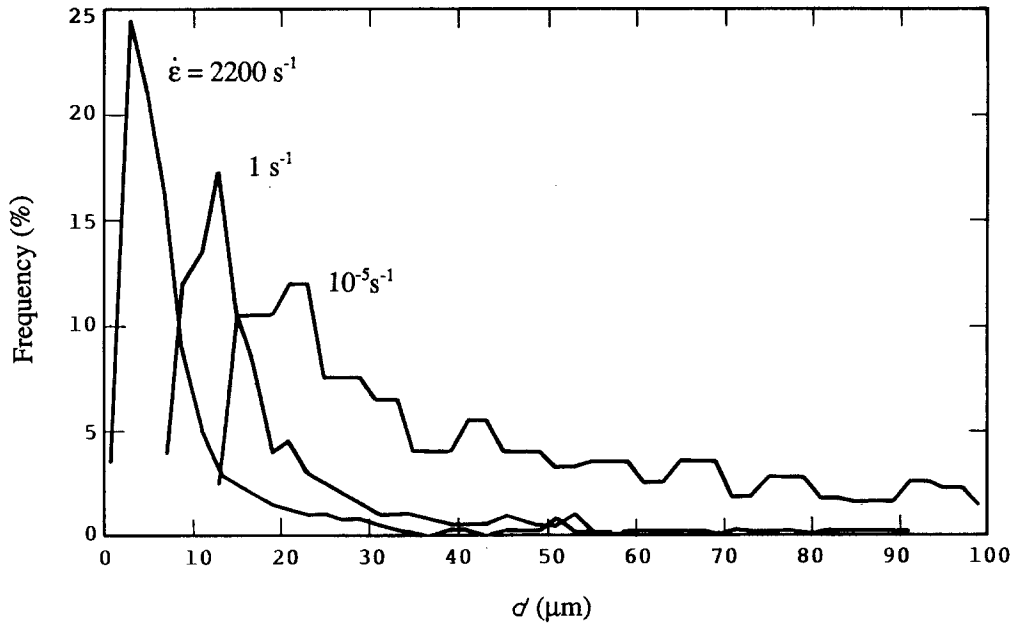

Figure 1 Frequency of size against fragment size for three strain rates; each distribution based on analysis of at least 2500 particles.

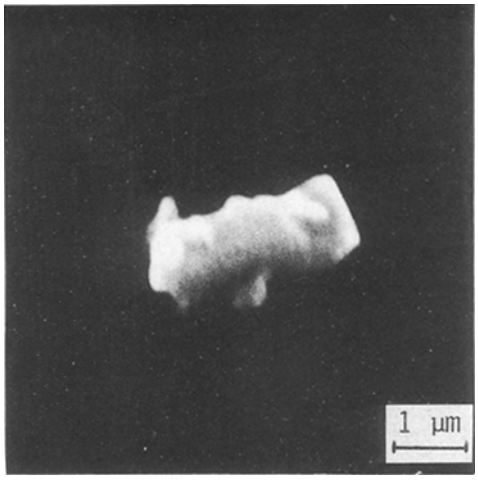

Figure 2 Typical SiC fragment representative of the lower end of the size distribution corresponding to $\dot{\varepsilon} = 2200\ s^{-1}$.

4. Discussion

In order to focus the following discussion, it is divided into two parts, a brief section dealing with strain rates below about $10^3\ s^{-1}$, and a longer one pertaining to fragmentation under dynamic loading conditions.

4.1. Fragmentation at $\dot{\varepsilon} \lesssim 10^3\ s^{-1}$

It has previously been demonstrated [14] that within this regime, the modest rate of increase in compressive strength with strain rate is caused by the inhibition of thermally-activated microfracture within local tensile enclaves. Thus, the reciprocal of the slope of $\log \sigma_c$–$\log \dot{\varepsilon}$ has been shown to equal (approximately) the slope of $\log K$–$\log V$ for a variety of ceramics, where V is the velocity of macroscopic tensile cracks subject to a stress intensity, K.

This being so, the effect of strain rate on fragment size can be rationalized as follows. As the strain rate increases, cracks nucleated at a given stress level have less time to grow, and so are accordingly smaller and less interactive at higher stresses. This prolongs failure and permits microcracks with higher nucleation stresses to introduce themselves into the microstructure. Failure ultimately occurs via the interaction and coalescence of a population of microcracks which, with increasing stress rate, is both more numerous and, at the same time, smaller in average size. The inevitable consequence of this process is smaller and more numerous fragments, because their boundaries are literally composed of coalescing microcracks.

4.2. Fragmentation at $\dot{\varepsilon} \gtrsim 10^3\ s^{-1}$

As noted earlier, there are several factors which may have an effect on the dynamic compressive strength and, possibly, the resultant fragment size of ceramics. These include dynamic lateral stresses, crack inertia, and plasticity-nucleated microfracture. Based on recent experiments [15] involving aluminium nitride, it seems unlikely that inertial confinement conditions are approached in the split Hopkinson bar. In particular, several variants of AlN were tested in compression over the strain rate range of the present study. All specimens at all strain rates failed by microcrack coalescence, i.e. virtual explosion into a multitude of fragments. Despite nominal similarities in the AlN variants, which differed principally in regard to starting powders, three of them evinced marked increases in strength for $\dot{\varepsilon} \simeq 10^3\ s^{-1}$, while two did not, but

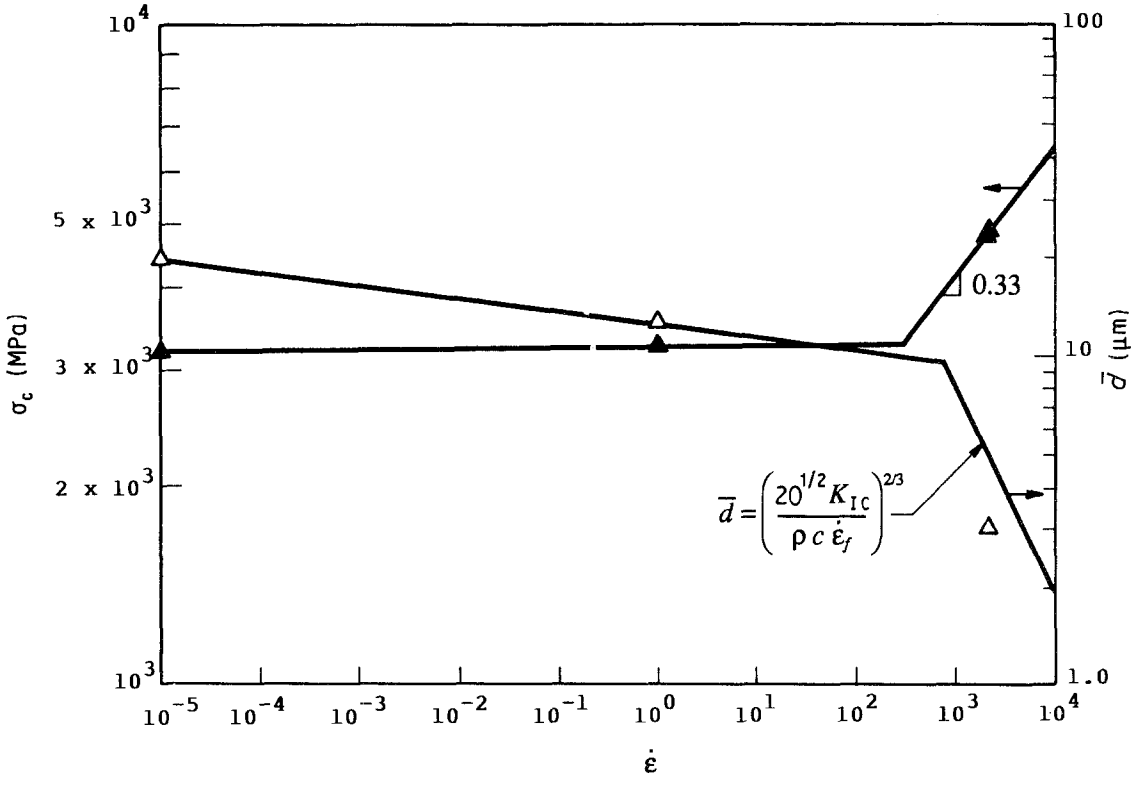

Figure 3 Compressive strength and corresponding peak frequency fragment size against strain rate.

rather fell precisely on the same plot which described the lower strain rate data. Yet, since the effective dynamic confining pressure is governed solely by elastic factors, all of the aluminium nitrides should have experienced essentially the same degree of strengthening due to inertial confinement.

Moreover, the SiC fragment size distribution itself is contrary to expectations based on confinement. In particular, the application of confining pressure requires only a higher uniaxial stress (to overcome the pressure and open up cracks closed by it); this does not alter the fundamental nature of the failure process itself, which should simply follow the lower strain rate, thermally activated trend discussed earlier. Thus, it would be expected upon extrapolating the latter to $\dot{\varepsilon} = 2.2 \times 10^3$, that $\bar{d}$ should be of the order of 10 μm, rather than the much smaller observed size of about 3 μm.

Crack dynamics concepts, however, predict failure strengths and fragment sizes which rapidly increase and decrease, respectively, with strain rate. In particular, it was shown that the fracture of a brittle material by the nucleation and growth of tensile microcracks under dynamic loads should scale with strain rate to the one third power (Equation 5). The relationship should be relevant to compression via the failure process discussed above, but the actual failure stress levels cannot be predicted numerically, because it is not known how to derive a general expression for the resolution of a nominal compressive stress field into microstructure-dependent tensile enclaves. Earlier work on sintered alpha silicon carbide [14] has demonstrated a near one-third power dependence for σ_c against $\dot{\varepsilon} \geqslant 10^3\ s^{-1}$. Based on those results, such a curve has been drawn through the present failure data (Fig. 2). The question of principal interest here is whether the same governing physics is reflected in fragment size. This issue can be addressed by inserting the appropriate parameters for SiC (Table I) into Equation 1, which yields the plot shown in Fig. 2. It is clear that the experimental result is in fair agreement with this relationship, but it is worth considering the possible significance of the fact that the prediction is on the high side.

In particular, another way of envisioning the dynamic fracture process is to recall that as the strain rate increases, the stress required to fail the specimen may rise to a level sufficient to induce plastic flow in the ceramic. Thus, the Hugoniot elastic limit (HEL) for SiC can be as low as 8 GPa [16]; this represents the stress level under uniaxial strain conditions necessary to produce macroscopic plastic flow. Based on preceding arguments, it is likely that these conditions, which effectively correspond to inertial confinement, are relaxed in split Hopkinson pressure bar experiments, so that the equivalent plastic flow limit would be that characteristic of uniaxial stress. The latter dynamic flow stress is related to the HEL according to [17]

$$\sigma_y^D = \frac{(1 - 2\nu)}{(1 - \nu)}\text{HEL} \tag{6}$$

Because $\nu = 0.21$ for SiC, the corresponding dynamic yield strength is only 6.1 GPa. This stress is just above that (4.8 GPa) achieved in the present high strain rate experiments. For properly oriented grains, plastic flow may occur in the latter regime.

In his plasticity-induced fracture work [11], Hagan envisioned dislocation pile-ups leading to Stroh-type [18] crack nucleation, which represents one of several basically equivalent [19] (in the present context) configurations leading to microcrack formation. Essential elements of the problem are shown in Fig. 4, in which dislocations have piled up under the influence of an applied shear stress, σ_s, along a slip length, L, at a barrier AB, such as a grain boundary. At some angle, θ, relative to the slip plane, tensile stresses, σ_t, caused by the pile-up are a maximum, their magnitude at a distance, r, being given by

$$\sigma_t = \sigma_s\left(\frac{L}{r}\right)^{1/2} f(\theta) \tag{7}$$

where $f(\theta)$ provides the angular dependence. As shown originally by Stroh [18], the dislocations in the pile-up will collapse and coalesce to form a crack along r when

$$\sigma_s = \left\{\frac{3\pi}{8}\left[\frac{\gamma\mu}{(1 - \nu)L}\right]\right\}^{1/2} \tag{8}$$

in which γ is the fracture surface energy, and μ is the shear modulus. In the present instance, it is assumed that yielding will occur once σ_s exceeds the dynamic shear strength, σ_s^D.

As pointed out by Stroh [18], and subsequently by Hagan [20], a crack nucleated at a pile-up according to Equation 8 can grow until its length is comparable to L, at which point it has exhausted its local driving force. Thus, to determine a typical size, $\bar{c}$, for such a crack, L in Equation 8 is equated with $\bar{c}$. Replacing $\gamma(= K_{IC}^2(1 - \nu^2)/2E)$ and $\mu(= E/2(1 + \nu))$, and solving for the crack length yields for dynamic stress levels approaching the HEL

$$\bar{c} = \frac{3\pi}{32}\left(\frac{K_{IC}}{\sigma_s^D}\right)^2 \tag{9}$$

where $\sigma_s^D \simeq \frac{1}{2}\sigma_y^D$. Substituting appropriate values for K_{IC} and σ_s^D yields a predicted plastic-flow nucleated crack size of 0.4 μm.

Recalling Fig. 1, it appears that the smallest observed particles are, indeed, of the order of 0.5 μm in size. The presence of such cracks, superimposed on the

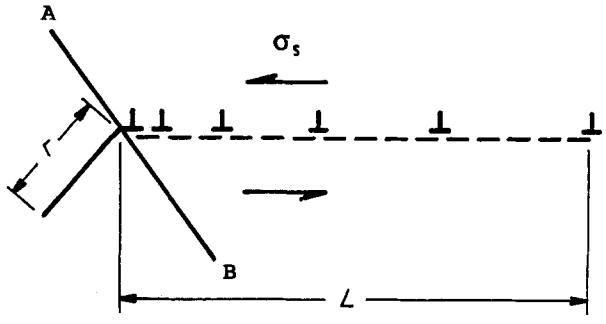

Figure 4 Schematic diagram of dislocations piled up over a distance L at a barrier, AB, producing a crack along r.

family of cracks related to "normal" dynamic microcrack initiation at intrinsic flaws, would necessarily lower the average fragment size as observed experimentally in Fig. 3. This would tend to produce fragments in the form of parallelepipeds, i.e. with long sides related to Equation 1, and shorter sides controlled by Equation 9. Fig. 2 is an example of just such a geometry.

The preceding scenario is represented schematically by curve (a) in Fig. 5, which includes the present SHPB data point. Here the dashed line delineates the strain rate corresponding to a uniaxial stress level equivalent to the dynamic yield point (HEL), assuming the validity of the σ_c–$\dot{\varepsilon}$ curve drawn in Fig. 3. Along curve (a), microcracks are forming at dislocation pile-ups in grains preferentially oriented such that the local stress level exceeds σ_y^D. As the strain rate increases, so does the overall stress level (Fig. 3), and the resultant population of dislocation nucleated cracks. The latter drives the average fragment size lower and lower, until at $\sigma_y = \sigma_y^D$, $\bar{d} \simeq 0.4$ μm, as predicted by Equation 9.

Curve (b), on the other hand, represents a situation in which there is essentially no sub-HEL microplasticity, hence, no associated microfracture; in this case, until $\sigma_c = \sigma_y^D$, $\bar{d}$ is governed by Equation 1. For still higher stresses, the fragment size is shown decreasing gradually, rather than dropping precipitously to $\bar{d} \approx 0.4$ μm. This reflects the physical requirement that there be sufficient dislocations per slip plane to produce the stress necessary to induce microfracture at the head of the pile-up. Elementary calculations based on the work of Stroh [18] are sufficient to indicate that for the present class of ceramics, about 200 dislocations would be required to satisfy this condition. If other nearby sources are activated prior to this point, or if slip should be initiated in adjacent glide planes, the pile-up stress may be insufficient to cause fracture. Thus, higher stresses (strain rates) would be required in order to raise gradually the population of microcracks, and correspondingly lower the average fragment size.

Finally, curve (c) represents a situation similar to this, but differing in that while plasticity is present for $\sigma_c > \sigma_y^D$, there is at first no corresponding microfracture. Eventually, with increasing stress and strain rate, sufficient dislocations are present on some of the slip planes for microcracking and associated fragmentation to begin. Subsequent development then parallels that indicated by curve (b).

Whether or not this scenario is true depends (at least) on whether dislocations actually are produced in ceramics under such impact loading conditions. In fact, a rather extensive literature [21–23] shows that explosively loaded ceramic powders are highly dislocated, and that such powders (Al_2O_3, SiC, MgO, B_4C) can be reduced to fragments of the order of 0.5 μm in size [21]; coherent crystallites within the fragments can be much smaller [22]. Somewhat more relevant to the present study, and seemingly consonant with the proposed notion of the sub-HEL, plasticity-with-associated-fracture, is the recent plate impact study by Louro and Meyers [24]. In this work, alumina flyer plates were subjected to transient compressive pulses of 4.6 GPA, against the measured HEL of 6.0 GPa. (This compares with the present SHPB experiments, in which SiC samples were fragmented in dynamic compression at stress levels of about 5.0 GPA, against HEL $\simeq$ 8.0 GPa.). Transmission electron microscopy of regions away from the spall plane revealed that the onset of damage corresponded to dislocations and intercrystalline microfracture, while the spall (failure) zone was primarily transcrystalline. The latter supports the possibility that its origin was precursory plasticity which, at higher stresses, nucleated transgranular microfracture/fragmentation. The possible sources of such shock-induced slip bands in crystalline solids has recently been explored theoretically by Coffey [25, 26]; he notes that the limiting consequence of their activity is microfracture at the tips of the bands, once they have attained a critical number of dislocations.

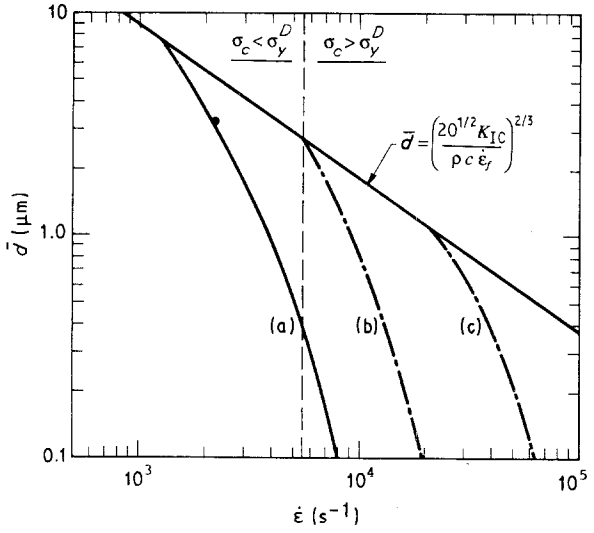

Figure 5 Schematic illustration of the range of effect of plastic flow-nucleated microfracture on fragment size: (a) local plastic flow and micro-cracking below general yield; (b) microcracking at onset of general yield; (c) microcracking above general yield point, corresponding to achievement of a critical number of dislocations per slip plane.

5. Conclusions

The fragmentation of SiC at strain rates above 2000 s^{-1}, and stress levels below the Hugoniot elastic limit, seems to be compatible with two concurrent dynamic damage mechanisms. The first is the development of microcracks at intrinsic microstructural flaws at a rate controlled by stress wave–flaw interaction kinetics. The second, more speculative, mechanism involves the possibility of microcrack nucleation at the heads of shock-induced dislocation planar arrays. Experiments at high strain rates are needed in order to permit the fragment size divergence which the two models predict to distinguish their relative contributions to the fragmentation process.

Acknowledgements

The authors thank A. Nicholls and J. Spencer for careful experimental work and the Office of Naval

Research for support under Contract no. N00014-84-C-0213.

References

1. D. E. GRADY, *J. Appl. Phys.* **53** (1982) 322.
2. D. E. GRADY and M. E. KIPP, *Int. J. Rock Mech. Min. Sci.* **17** (1980) 147.
3. M. E. KIPP and D. E. GRADY, *J. Mech. Phys. Solids* **33** (1985) 399.
4. W. JANACH, *Int. J. Rock Mech. Min. Sci. Geomech. Abstr.* **13** (1976) 177.
5. L. A. GLENN and W. JANACH, *Int. J. Fract.* **13** (1977) 301.
6. T. G. H. B. BODDY, *Nature* **54** (1943) 151.
7. B. M. PARRISH, *J. Appl. Phys.* **18** (1967) 233.
8. K. E. PUTTICK, *J. Phys. D* **12** (1979) L19.
9. K. KENDALL, *Proc. Roy. Soc.* **A361** (1978) 245.
10. B. L. KARLIHALOO, *ibid.* **A368** (1979) 483.
11. J. T. HAGAN, *J. Mater. Sci.* **16** (1981) 2909.
12. J. LANKFORD, *ibid.* **12** (1977) 2195.
13. D. E. GRADY and J. LIPKIN, *Geophys. Res. Lett.* **7** (1980) 255.
14. J. LANKFORD, *J. Amer. Ceram. Soc.* **64** (1981) C-33.
15. J. LANKFORD, unpublished data (1990).
16. W. H. GUST, A. C. HOLT and E. B. ROYCE, *J. Appl. Phys.* **44** (1973) 550.
17. Z. ROZENBERG and Y. YESHURUN, *Int. J. Impact Engng* **7** (1988) 357.
18. A. N. STROH, *Adv. Phys.* **6** (1957) 418.
19. A. S. KEH, J. C. M. LI and Y. T. CHOU, *Acta Metall.* **7** (1959) 694.
20. J. T. HAGAN, *J. Mater. Sci.* **14** (1979) 2975.
21. O. R. BERGMANN and J. BARRINGTON, *J. Amer. Ceram. Soc.* **49** (1966) 502.
22. B. MOROSIN and R. A. GRAHM, *Mater. Sci. Engng* **66** (1984) 73.
23. R. W. HECKEL and J. L. YOUNGBLOOD, *J. Amer. Ceram. Soc.* **51** (1968) 398.
24. L. H. L. LOURO and M. A. MEYERS, *J. Mater. Sci.* **24** (1989) 2516.
25. C. S. COFFEY, *J. Appl. Phys.* **62** (1987) 2727.
26. *Idem., ibid.* **62** (1987) 1654.

Received 29 May
and accepted 6 June 1990